JOURNAL OF MATERIALS SCIENCE 33 (1998) 1049–1055

Kinetics and phase evolution during carbothermal synthesis of titanium carbide from ultrafine titania/carbon mixture

R. KOC
Department of Mechanical Engineering and Energy Process, Southern Illinois University at Carbondale, IL 62901 USA

The kinetics and phase evolution of the TiC formation process by carbothermal reduction of ultrafine titania/carbon mixture were investigated using thermogravimetric analysis (TGA), X-ray diffraction (XRD) and oxygen analysis. Titania (TiO_2) first lowered its oxidation state to Ti_3O_5 via an unidentified phase (possibly one of the Magneli phases). Then Ti_3O_5 was further reduced to Ti_2O_3, followed by the formation of titanium oxycarbide (TiC_xO_y) phase and its purification toward high purity TiC thereafter. Ti_2O_3 was the oxide phase with the lowest oxidation state before forming TiC_xO_y phase. In the isothermal TGA trace, the formation of Ti_3O_5 showed a diffusion-controlled process; possibly carbon diffusion limited the solid state reaction. The formation of Ti_2O_3 and TiC_xO_y was interpreted to be associated with CO gas-assisted reduction reaction, based on constant reaction rate for each process. The activation energy for the formation of Ti_2O_3 (from Ti_3O_5) and TiC_xO_y (from Ti_2O_3) phase were calculated to be 415.6 and 264.3 kJ mol^{-1}, respectively. The TiC powder synthesized at 1550 °C for 4 h in flowing argon atmosphere showed fine particle size (0.3–0.6 μm) with oxygen content of 0.7 wt% and lattice parameter of 0.4328 nm while interparticle agglomeration was moderate.

1. Introduction

Titanium carbide is a ceramic material with many applications in key high technologies from mechanical to chemical and microelectronics because of its high melting point (3260 °C), high hardness (Knoop's = 32.4 GPa), high electrical conductivity (30×10^6 Ω^{-1} cm), high thermal conductivity (16.7 W mK^{-1}), high thermal shock resistance, high chemical stability, high wear resistance, and high solvency for other carbides [1]. Titanium carbide powder is used for the manufacture of cutting tools, grinding wheels and the like or can be combined with other ceramic systems such as aluminium oxide (Al_2O_3), silicon nitride (Si_3N_4) and silicon carbide (SiC) for the fabrication of structural components used in high temperature, erosive and/or corrosive applications [2–6]. Titanium carbide can also substitute for tungsten carbide (WC), a common machining material, because of its similar properties. Important benefit of the substitution results from the fact that WC requires cobalt as a binder material [7]. This binder is imported to the US from foreign and occasionally politically unstable sources. Titanium carbide compounds use nickel as a binder which has a more stable source and costs only half as much. For all these applications, the synthesis of titanium carbide powders with a homogeneous chemical composition, fine particle size, a narrow particle size distribution, and a loose agglomeration is of great importance.

Methods that have been developed to synthesize TiC powders include the direct carbonization of titanium metal (combustion synthesis) [8] or titanium hydride [9], gaseous pyrolysis of titanium halide such as $TiCl_4$ in a carbon containing atmosphere [7], and carbothermal reduction of TiO_2 with carbon in controlled atmospheres at high temperatures [3, 10]. Metallic titanium as a starting material is relatively expensive, and furthermore, the oxygen contained in the metal can hardly be reduced, so that the product is generally characterized by a high oxygen content [3]. Titanium chloride as a precursor is of importance in the field of chemical vapour deposition, but it is very expensive. An inexpensive method applied commercially involves the carbothermal reduction reaction of titania (TiO_2) and carbon particles [10].

In the carbothermal synthesis of titanium carbide from a mixture of carbon and titania, the overall reaction governing the formation of TiC is

$$TiO_2 + 3C = TiC + 2CO(g) \quad (1)$$

The reaction (Equation 1) is highly endothermic and proceeds above 1289 °C for a partial pressure of CO below 1.013×10^5 Pa. However, the actual titanium carbide production is achieved at much higher temperatures than the thermodynamic onset temperature because of kinetic barriers such as limited contact area between reactants and uneven distribution of carbon in the reactants. These limitations and higher

temperature processing result in grain growth, particle coalescence, non-uniform particle shape, and considerable quantities of unreacted TiO_2 and carbon in the final product. For example, in the commercial production of titanium carbide [10], reactants are fired at 1900 °C to 2300 °C in an inert atmosphere while sintered lumps of titanium carbide are produced. This then requires crushing using jaw crushers and fine-milling thereafter.

Of the number of efforts to develop the carbothermal processing of titanium carbide in the author's research group [11, 12], results based upon the use of the currently available ultrafine titania powder as the titanium source is reported herein. Such a fine powder would increase the homogeneity of the reactants and the high specific surface energy of the powder would result in decreasing the processing temperature. This would then ensure less chance of grain growth and particle agglomeration. While the development of carbothermal processing for titanium carbide requires fundamental research concerning the reactions, a number of inconsistencies in the phase evolution of titanium carbide formation are noticed in the literature. In the present study, the phase evolution and kinetics of carbothermal reduction of ultrafine titania/carbon powder mixture are established.

2. Literature review

While earlier works [13] proposed that the formation of titanium carbide by carbothermal reduction of titania/carbon proceeded via Ti_2O_3 and TiO, Samsonov [14] suggested that the reduction of titania proceeded through Ti_3O_5, Ti_2O_3, and TiO. However, Kucev and Ormont [15] concluded that the titanium carbide formation proceeded via Ti_3O_5, which in turn, resulted in titanium oxycarbide TiC_xO_y in excess of carbon or Ti_2O_3 in deficiency of carbon. On the other hand, Quensanga [16] came to the result that the lowest oxide of titanium existing in the system was Ti_3O_5 and the composition of initial TiC_xO_y was $x = 0.67$ and $y = 0.33$. According to Lyubirnov *et al.* [17], TiO_2 lowered its oxidation states to Ti_5O_9, Ti_3O_5, Ti_2O_3, TiO and Ti. While metallic titanium and TiO could not be detected on X-ray diffraction (XRD), their presence was drawn from chemical analysis results. Recently Berger [3] observed Magneli phases (Ti_nO_{2n-1} with n ranging between 4 and 10 [18]), various Ti_3O_5 modifications, and Ti_2O_3 on XRD while one of his carbon/titania mixtures showed a peculiar behaviour as the intermediate products Ti_3O_5 and Ti_2O_3 were missing. Concerning the lattice parameter of pure titanium carbide, different values have been reported, probably due to the difference in processing: 0.4328 [19] and 0.4331 nm [10].

3. Experimental procedure

Titania powder (titanium dioxide, P25, Degussa Corp., Ridgefield, NJ) used in this work had 70% anatase (30% rutile) phase, based on manufacturer's report. Its average particle size and specific surface area were reported to be 21 nm and 50–60 $m^2 g^{-1}$, respectively. The carbon source was carbon black powder (Monarch 880, Cabot, Waltham, MA) with an average particle size of 16 nm and specific surface area of 220 $m^2 g^{-1}$. A total of 10 g of titania 67.4 wt % and carbon black (32.6 wt %) powders were placed into a plastic container (inner diameter of 5 cm and height of 7 cm) and hand mixed using a spatula. Then two polymer balls (diameter of 0.35 cm) were added to the mixture in the plastic container and milled for five hours in a Spex mixer (model 8000 Mixer/Mill, Meutuchen, NJ).

For thermogravimetric analysis (TGA) (model TG-171, Cahn Instruments, Inc., Cerritos, CA), 0.2 g of the mixture was taken in a cylindrical graphite holder (internal diameter 1.25 cm and height 1.9 cm). The graphite holder was then placed in a cylindrical alumina holder (internal diameter 1.9 cm and height of 2.5 cm) with platinum hanger. The texture (sample, graphite holder, and alumina holder) was hung from a high precision balance. The B-type thermocouple, protected by an alumina tube, was placed at about 1 cm below the alumina sample holder. The system was surrounded by a perpendicularly positioned alumina tube furnace (internal diameter 3.2 cm). Argon gas was flowed from the bottom to the top for 6 h before increasing the temperature, and continued throughout the run. In order to minimize the degree of reaction before reaching the destination temperature, the maximum allowable heating rate of the instrument was applied for operation: 70 °C min^{-1} up to 1000 °C and then 20 °C min^{-1} for temperatures above 1000 °C. After reaching the destination temperature (1145–1350 °C), the sample was fired for 2 h followed by furnace cooling down to 1000 °C (at 10 °C min^{-1}) at which point the furnace power was turned off. Data acquisition was performed every 5 s to a computer disk.

The samples fired in the TGA instrument were subject to XRD (model DMAX-B, Rigaku Corp., Tokyo, Japan) analysis for the study of phase evolution using CuK_α radiation and a zero-background sample cell. Speed of scanning 2θ angle was from 27 to 80° at 2° min^{-1}.

For the production of titanium carbide powders, 20 g of the carbon/titania mixture (33.7 wt % carbon) were placed in a graphite boat and then the boat with sample was positioned in the centre of a horizontally positioned alumina tube furnace (Model CTF 17/75/300, Carbolite, Hope, Sheffield, UK) with an internal diameter of 70 mm. Argon gas was flowed for 2 h before increasing temperature and continued throughout the run (1 l min^{-1}: LPM). Temperature was increased (to 1300–1550 °C) at 4 °C min^{-1} heating rate followed by 2 h of soaking time. The sample was cooled at 4 °C min^{-1} down to 800 °C where the furnace power was switched off. The temperature reading was based on the B-type thermocouple located between the alumina tube and molybdenum disilicide heating element.

The lattice parameter, oxygen content, and morphology of the titanium carbide product were investigated using XRD, chemical analysis (LECO, St. Joseph, MI), and transmission electron microscopy

(TEM) (model H7100FA, Hitachi Inc., Tokyo, Japan), respectively. Oxygen was analysed by infrared detection in a LECO R0416DR oxygen determinator. The lattice parameter of the reaction products was determined by X-ray powder diffractometry with CuK_α radiation. For calibration of errors in scanning angle, submicrometre nickel powder was used as an internal standard. The samples (65 wt %) and internal standard (35 wt %) were mixed using mortar and pestle and then were scanned from 25 to 150° (2θ) with 0.5° min^{-1} scanning rate. The lattice parameter value a associated with each peak position was calculated and plotted as function of $\cos^2\theta$ [20] in order to determine the least square line of the data

$$a = a_0 + K\cos^2\theta \quad (2)$$

where a_0 is the extrapolated true value of a when θ approaches 90° and K is the slope of the least square line.

4. Results and discussion

4.1. Phase evolution

XRD results of the samples after passing through isothermal TGA analysis at various temperatures are shown in Fig. 1. After firing at 1145 °C for 2 h, Ti_3O_5 and unidentified peak intensities were observed with no evidence of TiO_2. The unidentified peak intensities are from phases (possibly one of the Magneli phases), with oxidation state between TiO_2 and Ti_3O_5 since such peak intensities disappeared at 1160 °C while Ti_3O_5 peak intensities grew. Further increase of temperature to 1175 °C resulted in the formation of Ti_2O_3 and TiC_xO_y (as will be shown later using lattice parameter data and oxygen content in Fig. 5, initial formation is not pure titanium carbide. It is in fact a solid solution of TiC and TiO with the virtual formula of TiC_xO_y). The XRD pattern at 1200 °C showed increase in the peak intensities of TiC_xO_y and decreased in that of Ti_2O_3, implying the growth of TiC_xO_y phase at the expense of Ti_2O_3. The lowest oxide phase before forming TiC_xO_y in the system was observed to be Ti_2O_3. At 1250 °C and above, only TiC_xO_y phase was present with no other phases (see Fig. 3).

4.2. Isothermal TGA results

Fig. 2 shows the isothermal TGA traces at various temperatures. The fraction of conversion α is based on the relation

$$\alpha = \%\ \text{wt loss/theoretical}\ \%\ \text{wt loss} \quad (3)$$

where the theoretical loss is 48.33 wt % based on Equation 1. In Fig. 2, the higher the reaction temperature, the greater the fraction of reaction occurring before reaching the firing temperature, resulting in the higher initial α values. This was the fact that a significant portion of reaction occurred while the sample was passing through a high temperature range (where reaction proceeded fast) before reaching the destination temperature. The weight loss of the carbon/titania mixture after the reaction indicated the degree

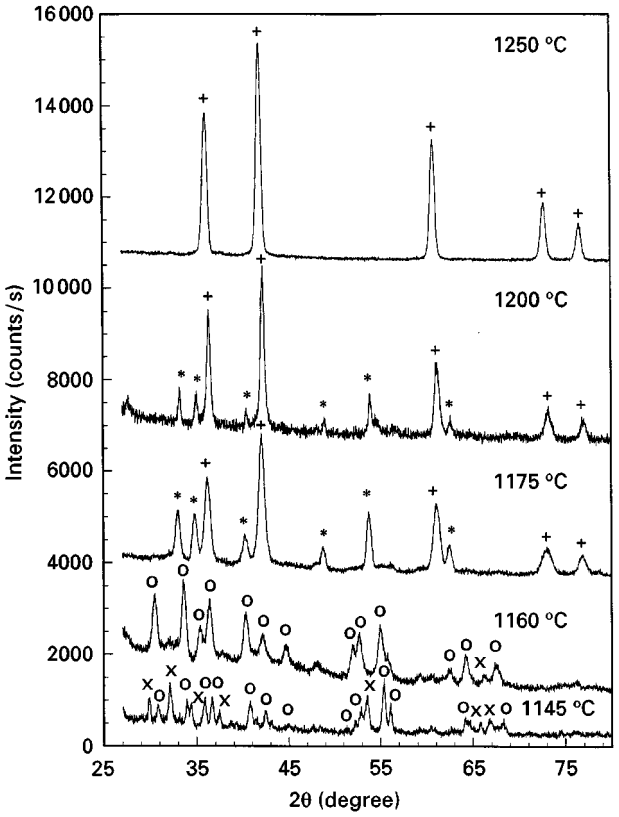

Figure 1 XRD results of reaction products from titania/carbon samples passed through TGA analysis (heat treatment for 2 h at various temperatures). (×) unidentified phase, (○) Ti_3O_5; (*) Ti_2O_3, (+) TiC_xO_y.

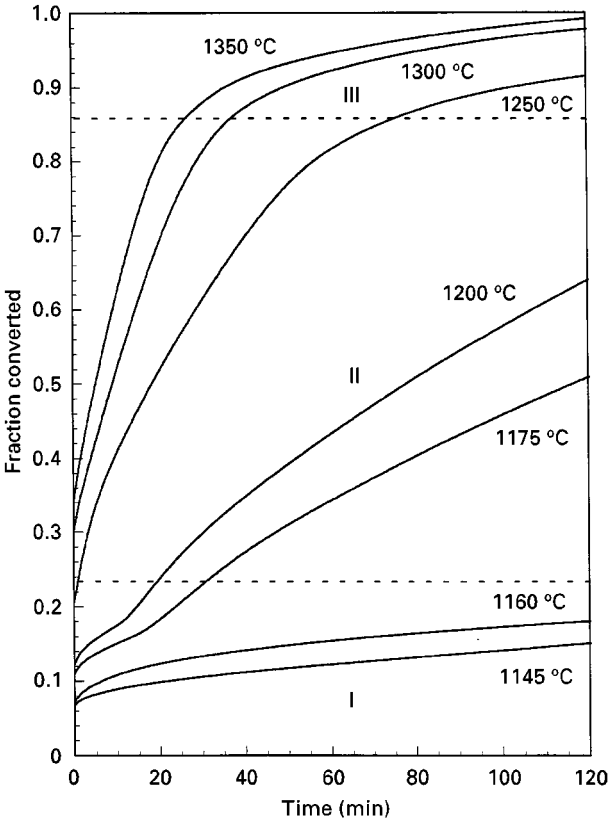

Figure 2 Isothermal TGA traces at various temperatures for titania/carbon samples.

of completion based on Equation 1. However, the calculation of isothermal reaction rate based upon the weight loss of sample after passing through heating–soaking–cooling certainly would lead to an erroneous result, unless the weight loss during heating and cooling would be properly compensated. The use of isothermal thermogravimetric analysis would reveal the evolution of isothermal reaction as a function of real reaction time after reaching the aimed temperature and hence is adopted in this work.

Combining Fig. 2 with the XRD results for 1145 and 1160 °C, the initial stage of the reaction is associated with the reduction of TiO_2 to Ti_3O_5. The possible initial stage reaction is

$$3TiO_2(s) + C(s) = Ti_3O_5(s) + CO(g) \quad (4)$$

where theoretical loss is 11.13 wt %, corresponding to an $\alpha = 0.23$. This is in agreement with the data in Fig. 2. This stage was characterized in terms of α: $0 \leqslant \alpha < 0.23$ as stage I.

Combining with the XRD results of 1175 and 1200 °C, the intermediate stage of the reaction is formation of Ti_2O_3 and TiC_xO_y from Ti_3O_5. The possible reactions for this stage are

$$a\,Ti_3O_5(s) + b\,C(s) = c\,Ti_2O_3(s) + d\,TiC_xO_y(s) + e\,CO(g) \quad (5)$$

$$a\,Ti_2O_3(s) + b\,C(s) = c\,TiC_xO_y(s) + d\,CO(g) \quad (6)$$

where theoretical loss could be as high as 41.22 wt %, corresponding to $\alpha = 0.85$. This is consistent with the observation in Fig. 1. There is a significant increase in the slope of this stage with increasing temperature, implying that this stage is a thermally activated process. Most of the weight loss occurs during this stage and resultant phases are Ti_2O_3 and TiC_xO_y, based upon the XRD patterns for 1175 and 1200 °C. This is determined to be stage II ($\alpha: 0.23 < \alpha \leqslant 0.85$). The significant increase in the slope for this stage are also attributed to gas–solid reactions instead of only solid–solid reactions as shown with Equations 5 and 6. This will be explained in detail in the next section.

The weight loss during the final stage is thought to be due to the purification process of TiC_xO_y phase toward TiC since no other phases were present at temperatures above 1250 °C. Fig. 3 shows XRD pattern of TiC synthesized at 1300–1500 °C for 2 h in flowing argon. Increased synthesis temperature results in increase for the TiC peak intensities, indicating a purer TiC product is being formed as more oxygen is eliminated.

In Fig. 2, three different stages are marked by combining the XRD results and the degree of slope. There are three stages during the carbothermal synthesis of TiC powders and determined in terms of α: $0 \leqslant \alpha < 0.23$ (stage I), $0.23 < \alpha \leqslant 0.85$ (stage II) and $0.85 < \alpha \leqslant 1.0$ (stage III).

4.3. Reaction mechanism

Based upon the shape of the TGA data in Fig. 2, stage I shows the characteristic of a diffusion controlled process ($\alpha = (kt)^{1/2}$, k = rate constant, t = time). The solid state diffusion of carbon, Equation 2, is the reaction mechanism for stage I. The sharp increase in the slope (Fig. 2) observed in stage II implys that this process may be a reaction-controlled process. Similar behaviour has also been observed during the carbothermal reduction of silica [21] where a gas phase (SiO) assisted reaction was recognized. Stage II is basically a reduction process. The solid state diffusion of the reducing agent carbon will not result in such a high reaction rate. Therefore, the reducing ability of CO via equilibrium of CO_2 gas is the proposed mechanism for such a reaction rate

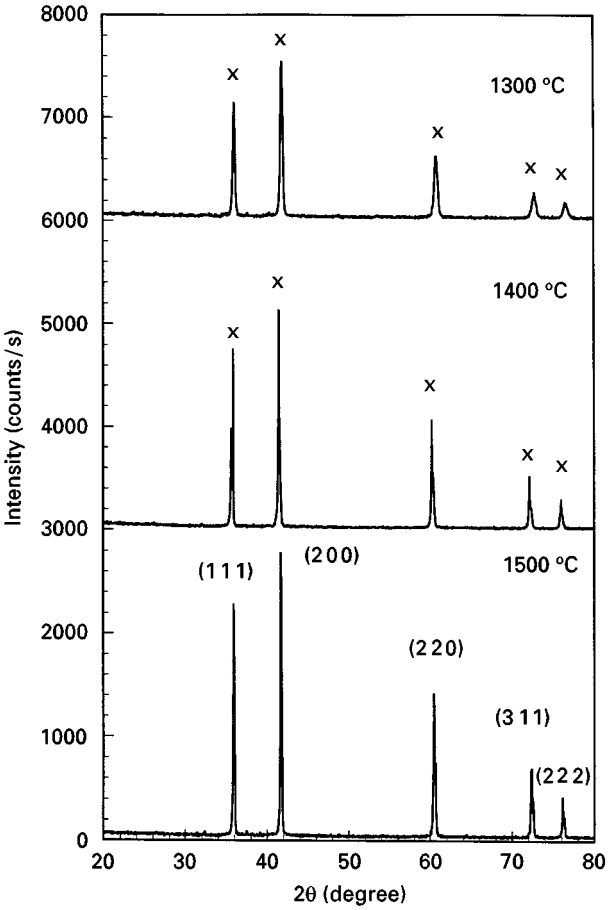

Figure 3 XRD results of titania/carbon black samples produced at 1300–1500 °C for 2 h in flowing argon at 1.013×10^5 Pa. $X = TiC_xO_y$.

$$2Ti_3O_5(s) + CO(g) = 3Ti_2O_3(s) + CO_2(g) \quad (7)$$

$$3Ti_2O_3(s) + 7CO(g) = 2TiC_xO_y(s) + 5CO_2(g) \quad (8)$$

where equilibrium CO_2/CO ratio is maintained via the reaction

$$CO_2(g) + C(s) = 2CO(g) \quad (9)$$

The CO_2/CO ratio must be governed by Equation 9, Ti_3O_5 reduction and TiC_xO_y formation by CO gas (Equations 7 and 8) it is thermodynamically favourable (Gibbs' free energy change of Equations 7–8 and 8–9 would be the same as their overall reactions (Equations 3 and 4), respectively). An increase in CO partial pressure, P_{CO} in the system favours Equations 7 and 8.

Overall reactions show that the Ti_2O_3 and TiC_xO_y formation are favoured by the decrease in P_{CO}. However, too low P_{CO} would lead to the reduction of titanium oxide by carbon instead of by CO. Because of this behaviour between the thermodynamic driving force (Equations 5 and 6) and kinetic processes (Equations 7–9), and intermediate P_{CO} is for stage II while a minimal P_{CO} fosters the progress of stage I.

These results indicated that the equilibrium state of the carbothermal reduction is both solid state (Equations 2, 5 and 6) and gas phase (Equations 7 and 8) reactions. Carbon is both a CO generator and a CO_2 reducer which keeps the CO_2/CO ratio low enough to make the reduction of TiO_2 possible by the gas phase reduction. The gas phase reactions are more favourable at low P_{CO}. This is because what is important in favouring the reduction reactions is CO_2/CO ratio rather than that of P_{CO} itself. Since the initial stage solid state reactions have low reaction rate, the intimate contact of carbon with oxides of titanium is most effective in reducing kinetic barriers.

The observed gradual decay of the reaction rate in stage III as compared to stage II implys the change of mechanism from a reaction controlled process (stage II) to a diffusion controlled one (stage III). Similar change of reaction rate has also been observed in the synthesis of SiC [21] where no purification of SiC was noticed. Hence, it is hard to correlate the trend (shape) of weight loss occurring at the final stage of total reaction with the mechanism of TiC_xO_y purification. Further work is required to uncover the detailed purification process of TiC_xO_y. While Equation 1 is the overall reaction for the carbothermal synthesis of TiC, it is not the reaction mechanism since TiO_2 is not observed to be present with TiC. Indeed Equations 2 and 5–9 describe the series of mechanisms of TiC formation by carbothermal reduction.

4.4. Activation energy

The reaction rate k of stage I and II were obtained from the linear slope of each stage. In order to obtain activation energy of the stages using the Arrhenius relation

$$k = A\exp(-\Delta E/RT) \tag{10}$$

a $\ln k$ versus $1/T$ plot is constructed in Fig. 4, where the slope corresponds to $-\Delta E/R$. In the Arrhenius relation, A is the pre-exponential constant, ΔE is the activation energy, and RT has its usual meaning. From Fig. 4, the activation energy for the stages I and II are calculated to be 415.6 and 264.3 kJ mol^{-1}, respectively.

According to the study of Binner *et al.* [22], activation energies of TiC formation from carbon/titania mixture were 56 and 63 kJ mol^{-1} for microwave heating and conventional heating, respectively. These values are very low as compared to the values obtained in this work and also low as compared to the formation of other carbides (by carbothermal synthesis) such as silicon carbide (from 251 to 552 kJ mol^{-1} depending upon raw materials and authors [23]) and boron carbide (301 and 820 kJ mol^{-1} depending on temperature range [24]).

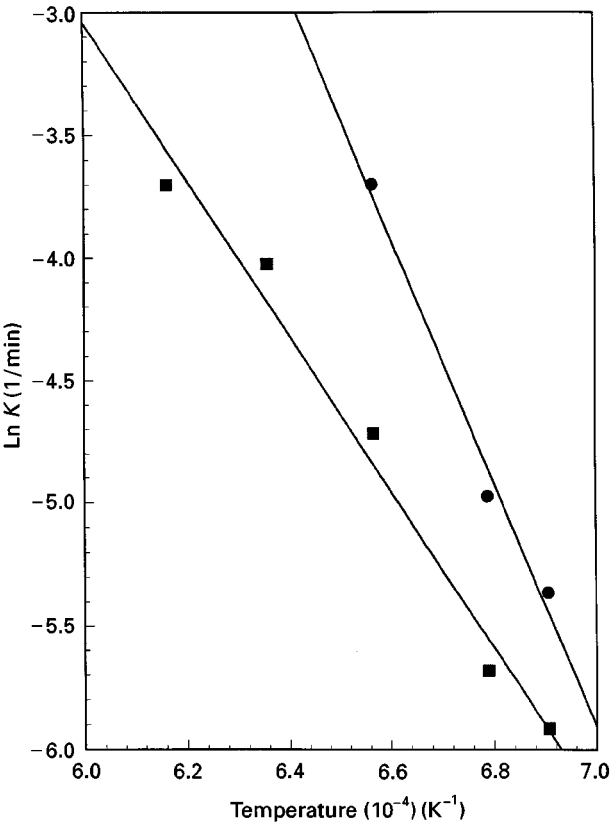

Figure 4 Arrhenius plot for stages I and II in Fig. 2. Stage I slope = − 209 928.6 kJ; stage II slope = − 133 518 kJ.

In Binner *et al.*'s work [22], the weight loss of the sample was measured after the sample passed through heating, soaking, and cooling. Then the reaction time was determined by counting soaking period plus half of the heating/cooling period above the onset temperature of the reaction (1050 and 1100 °C for microwave and conventional heating, respectively). Then the activation energy was calculated based upon the diffusion-controlled model by neglecting the individual reaction steps. The counting of half of the heating period was a highly rough approximation while counting the half of the cooling period was inappropriate because no significant reaction would take place during cooling as compared to heating. This was especially pronounced at higher temperature reaction and longer reaction period where not much reaction was left to complete during cooling. Hence, the higher the reaction temperature, more cooling time was counted, unnecessarily, as reaction time while less reaction was taking place during cooling. This resulted in the evaluation of less reaction rate k for higher temperature reactions. This then resulted in less temperature dependence of reaction rate k, which led into the low evaluation of the activation energy. As shown in Fig. 2, TiC formation in this work is multistep processes and cannot be treated as a single diffusion controlled mechanism.

4.5. Properties of synthesized TiC powders

Fig. 5 shows the change in oxygen content and lattice parameter of the TiC powder (produced using a horizontally positioned alumina tube furnace) as a

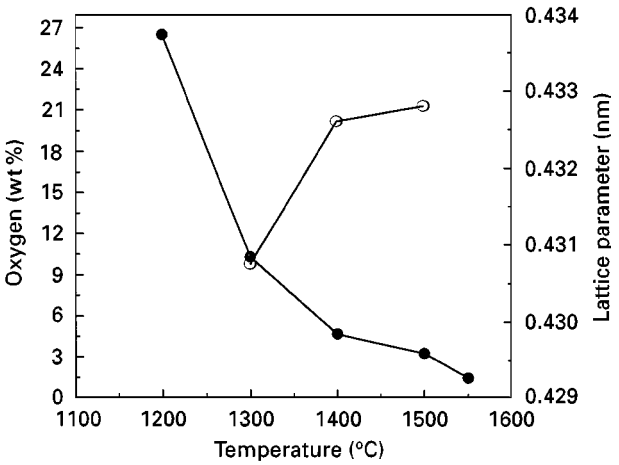

Figure 5 Change in oxygen content (●) and lattice parameter (○) of TiC powder product as a function of production temperature.

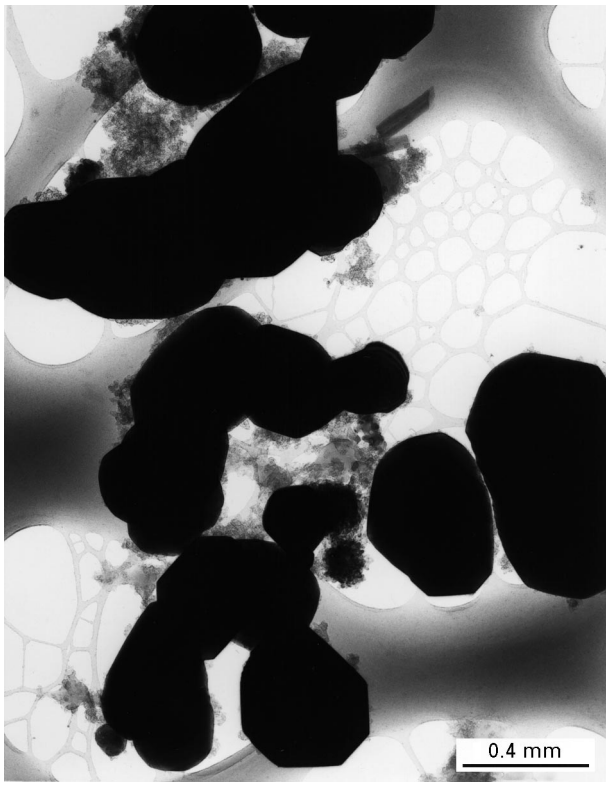

Figure 6 TEM micrograph of TiC powder synthesized at 1550 °C for 4 h in flowing argon.

function of reaction temperature. The lattice parameter increased with increasing temperature while the decrease in oxygen content was observed. Since oxygen and nitrogen are common impurities in TiC (up to as much as 50 at %) and are known to lower the lattice parameter of TiC [18], the observed low lattice parameters of reaction products with high oxygen content (at 1300 and 1400 °C) is because of the fact that TiC formed a solid solution with TiO [10, 19]. Fig. 5 implies that TiC_xO_y instead of pure TiC formed at lower temperature and then it is purified toward TiC at higher temperatures.

The morphology of the TiC powder synthesized at 1550 °C for 4 h is shown in Fig. 6. The TiC powders produced at 1550 °C for 4 h under flowing argon gas have oxygen content of about 0.7 wt %, a very fine particle size (0.3–0.6 μm) and are moderately agglomerated.

5. Conclusions

In the carbothermal synthesis of TiC from ultrafine titania/carbon mixture, titania first lowered its oxidation state via an unidentified titanium oxide phase to Ti_3O_5 followed by further reduction to Ti_2O_3 thereafter. Then TiC_xO_y grew from Ti_2O_3 followed by its purification toward pure TiC. The formation of Ti_3O_5 was shown to be a diffusion-controlled process, possible carbon diffusion-limited solid state reaction. Isothermal TGA results showed two linear stages associated with the formation of Ti_2O_3 and TiC_xO_y by CO gas-assisted reduction. Activation energy of each stage based upon Arrhenius relation were 415.6 and 264.3 kJ mol^{-1}, respectively. The TiC powder synthesized at 1550 °C for 4 h in flowing argon posses fine particle size (0.3–0.6 μm) with oxygen content of 0.7 wt % and lattice parameter of 0.4328 nm while interparticle agglomeration was prominent.

Acknowledgements

This research was sponsored by the US Department of Energy, Office of Industrial Technologies, as part of the Advanced Industrial Program, under contract DE-AC05-840R21400 with Lockheed Martin Energy Systems, Inc.

References

1. R. KAMO, "Adiabatic diesel engines", Engineered Materials Handbook, Vol. 4 (ASM International, Materials Park, PA, 1994) p. 990.
2. K. SUGANUMA, "Joining non-oxide ceramics", Engineered Materials Handbook, Vol. 4 (ASM International, Materials Park, PA, 1994) p. 529.
3. L. M. BERGER, *J. Hard Mater.* **3** (1992) 3.
4. Y. KATSUMURA, T. FUKATSU and M. KOBAYASHI, *Tribol. Trans.* **36** (1993) 43.
5. C. R. BLANCHARD and R. A. PAGE, *J. Amer. Ceram. Soc.* **73** (1990) 3442.
6. V. GROSS, J. HAYLOCK and M. V. SWAIN, *Mater. Sci. Forum* **34** (1988) 555.
7. D. D. HARBUCK, C. F. DAVIDSON and B. MONTE, *J. Metals* **38** (1986) 47.
8. D. C. HALVERSON, K. H. EWALD and Z. A. MUNIR, *J. Mater. Sci.* **28** (1993) 4583.
9. I. N. MIHAILESCU, M. L. De GIORGE, C. H. BOULMER-LEBORGNE and S. URDEA, *J. Appl. Phys.* **75** (1994) 5286.
10. R. DIVAKAR, K. Y. CHIA, S. M. KUNZ and S. K. LAU, in "Carbides", Encyclopedia of Chemical Technology, Vol. 4, edited by J. I. Kroschwitz and M. Howe-Grant (J. Wiley and Sons, New York, 1992) p. 841.
11. R. KOC and G. GLATZMAIER, US Patent No: 5,417,952 (1995).
12. R. KOC, *J. Eur. Ceram. Soc.* (1996) submitted.
13. G. A. MEERSON and J. M. LIPKES, *Russ. J. Appl. Chem.* **18** (1945) 251.
14. G. V. SAMSONOV, *Ukr. Khim. Zh.* **23** (1956) 287 (English Translation in Atomic Energy Commission-Technical Report 3387).
15. V. S. KUCEV and B. F. ORMONT, *Russ. J. Appl. Chem.* **29** (1955) 597.

16. A. OUENSANGA, *J. Less-Common Metals* **63** (1979) 225.
17. V. D. LYUBIMOV, S. I. ALYAMOVSKII and G. P. SHEVEIKIN, *Russ. J. Inorg. Chem.* **26** (1981) 1243.
18. J. L. MURRAY and H. A. WRIEDT, *Bull. Phase Diagrams* **8** (1987) 148.
19. E. K. STORMS, "The refractory carbides", Refractory Materials Series, Vol. 2 (Academic Press, New York, 1967) p. 1.
20. B. D. CULLITY, "Elements of X-ray diffraction", 2nd edn (Addison-Wesley Publishing Company, Inc., Reading, MA, 1978) p. 360.
21. J. G. LEE and I. B. CUTLER, *Am. Ceram. Soc. Bull.* **54** (1975) 195.
22. J. G. BINNER, N. A. HASSINE and T. E. CROSS, *J. Mater. Sci.* **30** (1995) 5389.
23. A. W. WEIMER, K. J. NILSEN, G. A. COCHRAN and R. P. ROACH, *AIChE J.* **39** (1993) 493.
24. A. W. WEIMER, W. G. MOORE, R. P. ROACH, J. E. HITT, R. S. DIXIT and S. E. PRATSINIS, *J. Amer. Ceram. Soc.* **75** (1992) 2509.

Received 12 September 1996
and accepted 5 August 1997